Electron-impact multiple ionization of Ne, Ar, Kr and Xe

2014 J. Phys. B: At. Mol. Opt. Phys. 47 105203

(http://iopscience.iop.org/0953-4075/47/10/105203)

IOP Publishing Journal of Physics B: Atomic, Molecular and Optical Physics
J. Phys. B: At. Mol. Opt. Phys. **47** (2014) 105203 (13pp) doi:10.1088/0953-4075/47/10/105203

Electron-impact multiple ionization of Ne, Ar, Kr and Xe

C C Montanari[1,2] **and J E Miraglia**[1,2]

[1] Instituto de Astronomía y Física del Espacio, Consejo Nacional de Investigaciones Científicas y Técnicas and Universidad de Buenos Aires, C1428EGA, Buenos Aires, Argentina
[2] Facultad de Ciencias Exactas y Naturales, Universidad de Buenos Aires, Buenos Aires, Argentina

E-mail: mclaudia@iafe.uba.ar

Received 28 January 2014, revised 26 March 2014
Accepted for publication 11 April 2014
Published 7 May 2014

Abstract

This work describes the multiple ionization cross sections of rare gases by electron-impact. We pay special attention to the high energy region (0.1–10 keV) where the direct ionization is a minor contribution and the post-collisional electron emission dominates the final target charge state. We report here electron-impact single to sextuple ionization cross sections and total ionization cross sections including direct and post-collisional processes, even in the total values. We use the continuum distorted wave and the first Born approximations adapted to describe light-particle impact, i.e. energy, mass and trajectory corrections are incorporated, the latter by considering the electron-target potential and by using the Abel transformation. Auger-type post-collisional contributions are included in the multinomial expansion through experimental branching ratios after single ionization events. Tabulations of these experimental branching ratios for all the orbitals of the four targets are included. Present results are compared with the large amount of electron-impact experimental data available. We have obtained a good description of the multiple-ionization measurements at high energies, where the post-collisional ionization dominates. At intermediate energies, our theoretical results show the correct tendency, with the electron-impact ionization cross sections being far below the proton-impact ones.

Keywords: multiple ionization, electron, post-colisional

1. Introduction

Electron-impact ionization is one of the most fundamental processes in atomic collisions and a very active field, both theoretically and experimentally ([1] and references therein). In the last 20 years, important developments have been made to solve the three- and four-body problem, such as the convergent close-coupled method, the *R*-matrix method with pseudo-states, the exterior complex scaling, or the time-dependent close-coupling method (reviews in [2–4]). These sophisticated methods have great accuracy and high computational requirements too.

When dealing with many-electron targets, moreover, when multiple ionization (MI) is the primary focus, these methods are still far from being applicable. We have to evaluate the physical problem and variables and to appeal to other approximations. In the intermediate and high energy regime, different approximations within the independent particle model (IPM), such as the continuum distorted wave methods [5, 6] or even the first Born approximation and its variants [7], provide good results within their ranges of applicability, and the advantage of working with considerable economy of computational resources and a more accessible and friendly description of the physics involved. In this line, we should mention the work by Bartlett and Stelbovics [7], who calculated total ionization cross sections by electron-impact for all the non-relativistic atoms of the periodic table using the first Born approximation. By following the IPM, we give up obtaining precise multi-differential cross sections at the deepest level.

MI processes arising in electron–atom and ion–atom collisions [8] play an important role both in the basic understanding of the many-electron problem in atomic physics (multiple-electron transitions, electron correlation effects,

collisional and post-collisional electron emission) and in different applications such as charge-state distributions of ions in plasmas and other environments with an abundance of energetic electrons.

By far, most of the MI experimental data on rare gases corresponds to electron impact, since the experimental works by Schram *et al* [9–11] in the 1960s to date [12–22]. MI measurements reveal the interest not only in neutral targets, but also in charged ions [23–25]. Semi-empirical formulations have been proposed by Fisher *et al* [26], Deutsch *et al* [27], and more recently by Shevelko *et al* [28, 29] with good results for a variety of neutral atoms and positive ions. Some attempts to introduce post-collisional ionization (PCI) in MI by electron impact combine the ionization cross sections of the different shells [30, 31]. However, no comprehensive theoretical description has succeeded in describing the high energy q-fold MI data for the different rare gases.

The goal of the present work is to present a comprehensive strategy to describe MI (single to sextuple) of the rare gases (Ne, Ar, Kr and Xe) in an extended energy range, covering the high energy region where PCI—due to relaxation and shake-off processes—is the main contribution.

We introduce PCI within the IPM following [32, 33], by using a formalism that has been successful for MI by heavy-projectile impact (ions of different charge states [34, 35], protons [36, 37] and antiprotons [38]). This formalism is valid within the IPM.

Our calculations are based on the continuum distorted-wave eikonal initial state (CDW-EIS) [39–41] and the first Born approximations for the ionization probabilities as a function of the impact parameter, adapted from heavy to light-particle impact. A similar methodology may be combined with any electron impact ionization model as long as reliable probabilities as a function of the impact parameter can be obtained.

In section 2 we will present the physical considerations to change from heavy to light-particle collisions and how these changes influence not only the single ionization probabilities but also the multiple ones. Finally, in section 3 the results for single to sextuple ionization, and for total ionization cross sections of the Ne, Ar, Kr and Xe are displayed and analysed in comparison with the experimental data.

2. Multiple ionization by light-particles

2.1. From heavy to light-particle collisions

Although this work is focused on electron-impact ionization, the theoretical strategy described in this section applies for both, electron and positron impact. The key point of this approach is to adapt previous heavy-ion atom calculations (proton and antiproton-impact) [38] by including the basic physics of light-particle collisions (mass, energy and non-straight line trajectories).

We start from the antiproton and proton T-matrix elements, $T^{\pm}_{nlm}(\eta)$, as a function of the transversal momentum transfer η, where nlm is the initial state, and $\pm$ indicates the sign of the incident heavy projectile. For each nlm-state a central potential V_{nlm} is determined from the Hartree–Fock wave functions. The initial (bound) and final (continuum) wave functions were obtained through the numerical solution of the same radial Schrödinger equation [42] and therefore they are fully orthogonal to each other. The continuum electron wave functions are expanded in the product of spherical harmonics [42], with maximum angular momentum $l_{\max} = 28$. We use around 70 values of η, 28 angles and around 45 electron energies. These $T^{\pm}_{nlm}(\eta)$ elements for heavy ion–atom inelastic collisions are the *seeds* to get the transition amplitudes as a function of the impact parameter for electron and positron impact, as described below.

In what follows we describe the physical considerations to go from heavy-particle T-matrix elements to light-particle MI probabilities, including direct and post-collisional ionization: the charge effect, the mass effect in the maximum momentum transfer and in the energy transfer, the non-straight line trajectory and the energy restriction to the MI.

2.1.1. The charge effect. The CDW-EIS approximation assures that the charge effect is taken into account from the very beginning. High-order terms in the projectile charge are included, at least approximately, and clearly, different values for $Z_P = \pm 1$ are obtained [38]. At very high impact velocity the results are independent of the charge sign and the first Born approximation holds, namely: $T^{\pm}_{nlm}(\eta) \to T^{\rm Born}_{nlm}(\eta)$.

2.1.2. The mass effect in the maximum transversal momentum transfer. The momentum transfer $\vec{q} = \vec{k}_i - \vec{k}_f$ can be decomposed in a parallel component to the incident velocity, $\vec{q}_z$, plus a perpendicular one, $\vec{\eta}$, so that $\vec{q} = \vec{q}_z + \vec{\eta}$. The minimum momentum transfer for heavy particles is $q_z = \Delta/v_i$, with $\Delta = \varepsilon_f - \varepsilon_i$, and ε_i, ε_f the initial binding (negative) energy of the electron under consideration and the final electron (positive) kinetics energy in the continuum, respectively. Within the eikonal approximation the ionization probability as a function of the impact parameter is obtained as

$$P^{\pm}_j(\vec{b}) = \left| \int \frac{\mathrm{d}\vec{\eta}}{2\pi} \exp(\mathrm{i}\vec{\eta}\cdot\vec{b})\, T^{\pm}_j(\vec{\eta}) \right|^2, \quad j = nlm, \quad (1)$$

For heavy projectiles, as protons or antiprotons, the integration over η extends to infinity. Instead, for light particles the maximum momentum transfer in (1) is estimated as

$$\eta_{\max} = k_f \approxeq \sqrt{k_i^2 - 2\Delta}. \quad (2)$$

2.1.3. The mass effect in the energy transfer. At equal velocities, the difference from heavy to light-particles is the impact energy, which should be at least larger than the ionization threshold of the active electron. We introduce the Heaviside step function $\Theta(v^2/2-\Delta)$ as a filter, i.e. the electron final kinetic energy, ε_f, must be smaller than $v^2/2 - |\varepsilon_i|$, otherwise the ionization cannot take place.

Following the previous two steps we build the impact parameter probabilities as

$$P^{(m)\pm}_j(\vec{b}) = \left| \int \frac{\mathrm{d}\vec{\eta}}{2\pi} \exp(\mathrm{i}\vec{\eta}\cdot\vec{b})\, T^{\pm}_j(\vec{\eta})\, \Theta(v^2/2-\Delta)\Theta(\eta-\eta_{\max}) \right|^2 \quad (3)$$

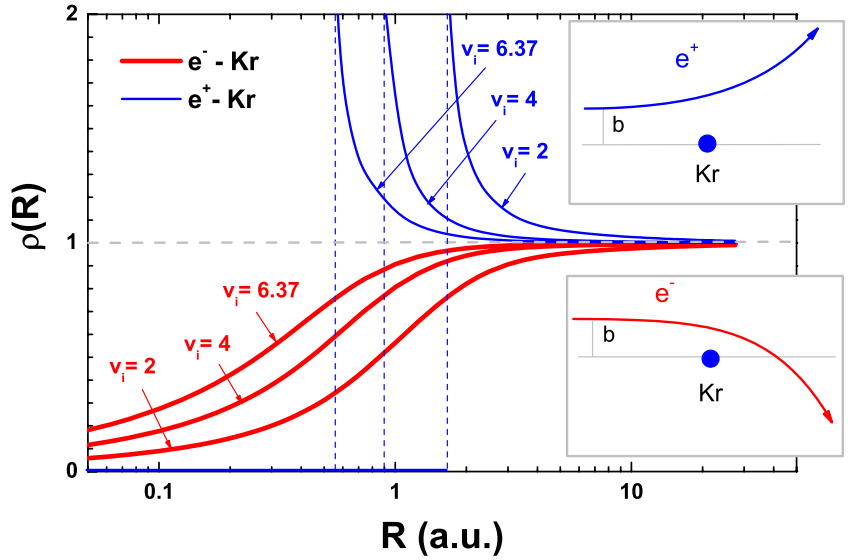

Figure 1. Visiting function given by (7) for electron and positron impact on Kr. The different impact velocities are indicated within the figure. The insets represent the electron e^- and positron e^+ trajectories.

where the superscript m indicates that we have introduced the mass correction for light particles. This mass correction is very important in the intermediate energy region where electron-impact cross sections clearly differ from proton-impact ones, and it is drastic for low energies for which electron-impact does not allow ionization at all.

2.1.4. The inclusion of the trajectory through the Abel transformation. While heavy particles describe essentially straight line paths, light particles are significantly deviated by the target. The trajectory is governed by the projectile-target potential, $V(R)$, as a function of the distance R between them.

Our next task is to incorporate the effect of the trajectory within the probabilities $P_{nlm}^{(m)\pm}(\vec{b})$ given by (3). To that end, we appeal to the Abel transformation. The probability can be written as

$$P_j^{(m)\pm}(b) = \int_{-\infty}^{+\infty} \mathrm{d}z\, W_j^{\pm}(R) = 2\int_b^{\infty} \mathrm{d}R\, R \frac{W_j^{\pm}(R)}{\sqrt{R^2-b^2}}. \quad (4)$$

where $R = \sqrt{b^2+z^2}$, $z = v\,t$, v is the incident velocity, and t is the time. This is the well known Abel transformation. The anti-transformation is given by

$$W_j^{\pm}(R) = -\frac{1}{\pi}\int_R^{\infty} \frac{\mathrm{d}b}{\sqrt{b^2-R^2}} \frac{\mathrm{d}}{\mathrm{d}b} P_j^{(m)\pm}(b). \quad (5)$$

If we ascribe to $W_j^{\pm}(R)$ the meaning of ionization probability as a function of the projectile-target distance R, then we are able to impose the effect of the trajectory by appealing to the classical micro-canonical assembly. Let us consider a classical particle of charge Z_P, mass m_P and kinetic energy $K = p^2/(2m_p)$, in a central potential $V = V(R)$. The position–momentum distribution in the phase space is given by

$$\rho(\vec{p}\,;\vec{R}\,) = C\,\delta(E-K-V), \quad (6)$$

where C is a normalization constant. Asymptotically $V(R\to\infty) \to 0$ and the total energy is just the incident kinetics energy $E = \frac{1}{2}m_p v^2$. Integrating over $\vec{p}$ we obtain

$$\rho(R) = \frac{v}{\sqrt{v^2 - \frac{2}{m_P}V(R)}}, \quad (7)$$

Table 1. Coefficients a_j and b_j for Ne, Ar, Kr and Xe in equation (8).

Atom	a_1	a_2	a_3	a_4	b_1	b_2	b_3	b_4
Ne	0.413	7.133	1.454	0.000	0.524	2.123	6.605	0.000
Ar	5.954	7.785	3.261	0.000	11.067	3.003	9.151	0.000
Kr	8.467	22.306	4.226	0.000	1.109	3.774	16.272	0.000
Xe	4.270	27.172	19.295	2.262	0.682	2.233	8.085	30.504

for R so that $\frac{1}{2}m_p v^2 > V(R)$, and $\rho(R) = 0$ elsewhere (exclusion zone). We have chosen the constant C to recover the scattering conditions $\rho(\vec{R}\,) \to 1$ when $R \to \infty$. Physically $\rho(R)$ is a *visiting function*; it states for the probability of the projectile to visit the position R. If we consider a heavy projectile, when $m_P \to \infty$, then $\rho(R) \to 1$. It means that the projectile samples all the positions of the space. For light particles this is not the case.

The shape of the *visiting function* depends on the interaction potential. For the four targets studied here, Ne, Ar, Kr and Xe, we estimate this potential using the code of the optimized potential model developed by Talman and co-workers [43], which includes exchange. For practical purposes we fitted these potentials with exponentials as

$$V(R) = \frac{Z_P}{R}\left(1 + \sum_i a_i \exp(-b_i R)\right), \quad (8)$$

with the coefficients a_i and b_i for Ne, Ar, Kr and Xe being included in table 1. Note that in (8) we consider the potential created by the positive ion (the nucleus and the passive electrons), the active electron has already been considered in the ionization calculation.

To illustrate the importance of $\rho(R)$ given by equation (7) we analyse the case of Kr. Figure 1 displays the *visiting function* for positron, $\rho^+(R)$, and electron impact, $\rho^-(R)$, at different asymptotic velocities, and the trajectory in both cases (repelled or attracted). In this figure we can immediately recognize the exclusion zone for the positrons, i.e. $\rho^+(R) = 0$ for $R < R^+$, so that $V(R^+) = \frac{1}{2}m_P v_i^2$. Conversely, electrons accelerate near the nucleus.

We then recover the ionization probability as a function of the impact parameter by using the Abel-transformation of the now-corrected probability

$$P_j^{(t,m)\pm}(b) = 2\int_b^\infty R\,\mathrm{d}R\,\frac{W_j^\pm(R)}{\sqrt{R^2-b^2}}\;\rho^\pm(R) \tag{9}$$

where $W_j^\pm$ is given by (5). The superscript t in (9) indicates the trajectory correction.

As figure 1 shows, electrons accelerate and $\rho^-(R)$ diminishes for small R. This effect is stronger as the impact velocity decreases. By including this in (9) we can say that trajectory considerations make the small impact-parameter probabilities smaller for electron-impact than for heavy projectiles. Instead, for large impact-parameters they are not affected. As the MI probability is based on the product of probabilities, then the trajectory considerations will make it decrease considerably for small impact parameters.

2.1.5. The energy restriction to multiple ionization. The next step is to calculate the multiple processes. We distinguish the direct (or collisional) MI from the post-collisional one, in general due to inner-shell ionization followed by Auger-type processes.

Within the IPM, the probability of direct MI is obtained as a multinomial distribution of the ionization ones [32]. The probability of direct k-fold ionization (exactly k target electrons are removed) is obtained by the multinomial combination of ionization probabilities of exactly q_j electrons of each j-subshell, so that $k = \sum_j q_j$, as follows

$$\mathsf{P}_{(k)}(b) = \sum_{q_1+q_2+\ldots=k}\;\prod_j P_{(q_j)}(b), \tag{10}$$

and

$$P_{(q_j)}(b) = \binom{N_j}{q_j}[p_j(b)]^{q_j}[1-p_j(b)]^{N_j-q_j}, \tag{11}$$

where N_j is the total number of electrons in the j-subshell, and $p_j(b)$ is the ionization probability as a function of the impact parameter. In this work $p_j(b) = P_j^{(t,m)-}(b)$ as given by (9).

By using the IPM, the ejected electrons ignore each other: there is no two-step-one (TS1) possibility [44, 45]. MI within the IPM is seen as a multiple kick process in a very simplified scheme of an n-step-n process in which the projectile can collide with n electrons with no sequence at all. This leads to an incoherent product of probabilities.

Depending on the impact energy some inner-shell vacancies cannot be produced due to the third correction (impact energy below the ionization threshold). However, even if the impact energy is enough for single ionization, it may not be sufficient to transfer twice or three times that energy. The restriction in energy is stronger than the one expressed in (3) and should be included in the multinomial distribution. If $\sum \varepsilon_j$ is the total energy to remove q_j electrons from different j-subshells so that $q_1 + q_2 + \ldots = k$, then

$$\mathsf{P}_{(k)}^{(E)}(b) = \sum_{q_1+q_2+\ldots=k}\;\prod_j P_{(q_j)}(b)\;\Theta\left(v^2/2 - \sum\varepsilon_i\right). \tag{12}$$

The orbital binding energies ε_j correspond to our Hartree–Fock initial wave functions. As in the previous steps, this energy restriction also contributes to make MI by light particles to fall down in the intermediate energy range. The energy cutoff in MI is a key point, and proved to be decisive in the decrease of the experimental values of MI as will be shown later in this work.

To be consistent with the IPM, our ionization thresholds correspond to the binding energies of the neutral atom. No correction is performed to consider changes in this threshold when two, three or more electrons are removed; neither to take into account the kinetic energy of the emitted electron, which would require considering the sequence in which the electrons are removed. This means that the energy cutoff employed here is the *minimal* value it can take. This is an important point when we compare it with the experiments: our theory always runs above the experimental data in the low energy range.

In that respect, it is known that electron–electron correlation is important at low energies and the IPM cannot describe the vertical drop of experimental values in the energy region close to the appearance energy, AE, (the lowest possible energy for each k-fold MI). The k-fold MI cross sections close to the AE can be approximated as a power law of the excess electron energy above the threshold, with certain exponent p, which is expected to be around the number of ionized electrons [46, 47]. We will note later in this work that the low experimental values for this exponent are reasonable considering the PCI. Anyway, it should be said that the low energy behaviour is far outside the validity range of our theoretical approach.

2.2. Post-collisional multiple ionization

When an electron is emitted from a sub-valence shell, a vacancy is created and there is a not-null probability for different PCI processes giving rise to a higher target charge state. It is reasonable to consider that PCI is a time-delayed electron emission and, therefore, independent of the projectile. The Auger transitions of an autoionizing state are related to coupling of discrete and continuum states [48].

The experimental and theoretical work on post-collisional electron emission provides detailed distributions of the different channels that contribute to each final charge state. The inclusion of PCI within MI needs less detailed information, just the branching ratio of charge state distribution $F_{j,k}$, with j being the orbital of the initial single vacancy and k the number of electrons emitted in PCI.

Following previous works [37, 38] we use this unitarity of the branching ratios (i.e. $1 = \sum_{k=0}^{k_{\max}} F_{j,k}$) to introduce them in (11) as

$$P_{(q_j)}(b) = \binom{N_j}{q_j}\left[p_j(b)\sum_{i=0}^{i_{\max}} F_{j,i}\right]^{q_j}[1-p_j(b)]^{N_j-q_j}. \tag{13}$$

The MI probabilities including direct and PCI are obtained by replacing (13) in (12), expanding the different terms and putting together those that end in the same number of final emitted electrons (details in section 2.3 of [37]). This rearrangement gives rise to $\mathsf{P}_{(n)}^{\mathrm{PCI}}$, the probabilities of exactly n emitted electrons, part of them in direct ionization and part in PCI.

Within the electron-impact MI, the work by Singh and coworkers [21] for high energy electron-impact on Ar is the closest to the present proposal. Singh *et al* [21] add sub-shell ionization cross sections weighted with Carlson branching ratios [49].

The k-fold ionization cross section including PCI is

$$\sigma_k^{\rm PCI} = \int \mathrm{P}_{(k)}^{\rm PCI}(b)\, 2\pi\ b\ \mathrm{d}b. \tag{14}$$

By adding the k-fold ionization cross sections (with k being the final charge state of the target) we obtain the so-called *count* cross sections, related to the total number of final positive ions

$$\sigma_{\rm count} = \sum_k \sigma_k = \sum_k \sigma_k^{\rm PCI}. \tag{15}$$

As shown analytically in [38], the *count* cross sections remain unchanged at the inclusion of PCI. Instead, PCI does affect the total or *gross* sections (which measure the total number of emitted electrons)

$$\sigma_{\rm gross} = \sum_k k\, \sigma_k^{\rm PCI} \neq \sum_k k\, \sigma_k = \sum_{nlm} \sigma_{nlm}. \tag{16}$$

The lack of PCI in the total ionization cross sections leads to an underestimation of the experimental data. This issue is important in three respects. First, because measured gross cross sections $\sigma_{\rm gross}^{\rm Exp}$ do include PCI. Second, because total ionization has been much more studied than MI, both experimentally [10, 50–52] and theoretically (a vast literature, two examples in [7, 53]), so the comparison must be very clear. Third, because $\sigma_{\rm gross}^{\rm Exp} \neq \sum_{nlm} \sigma_{nlm}$.

Sometimes the total ionization cross section has been named indistinctly for *gross* or *count* cross sections. For example, the recent and very precise experimental data by Sorokin *et al* [54] are *count* cross sections. As a matter of fact, *count* cross sections are very interesting for the theoretical-experimental comparison because they are independent of PCI.

When we consider only direct MI, the theoretical values for *count* and *gross* cross sections are very close. Even taking into account PCI, theoretical *count* and *gross* cross sections for Ne or Ar differ less than 10% (see table 1 in [38]). But for Kr and Xe, this difference reaches 25% and 35%, respectively, at impact velocity $v = 20$ au [38]. This difference is well-known, de Heer *et al* [52] tabulated the experimental ratio *count/gross* for electron-impact ionization. We checked that our high energy values for this ratio are in good agreement with the recommended values by de Heer *et al* [52].

2.3. Branching ratios of multiple ionization

Following [32, 33, 37, 38], post-collisional MI is included using the accurate experimental data of single-photoionization ending in multiple-charged ions. While collecting these experimental values two points must be ensured: the sub-shell of the initial vacancy and that it is a single ionization followed by PCI (not double or triple photoionization, for example). In this way final target charge states can be attributed to post-collisional events.

Carlson, Krause and co-workers have been pioneers in the experimental and theoretical studies on multiple photoionization [49, 56–59]. They use x-ray tubes to get photons in a certain energy range close to that of the initial vacancies, so these measurements include outer-shell ionization too. The advent of the new experimental techniques in photoionization research brought a breakthrough in this field. Coincident measurements allow the total yield of Auger-electron emission processes to be accurately determined for vacancies in different shells of various atoms and multiple-photoionization to be separated from single-photoionization followed by PCI (see the compilation of the literature in tables 2, 3 and 4). However, it is fair to note that the earlier measurements by Carlson and collaborators in the 1960s, corrected to exclude outer-shell ionization, are in good agreement with recent ones using COLTRIMS techniques (see for example the corrected values by Krause *et al* [56] for Kr,

Table 2. Branching ratios for multiple ionization of Ne and Ar. $F_{j,i}$ is the yield of single photoionization of the j-subshell followed by the post-collisional emission of i electrons from outer shells, with the final charge state being $i + 1$.

	Ne			**Ar**				
	1s[a]	**2s**[b]	**2p**[b]	**1s**[c]	**2s**[d]	**2p**[d]	**3s**[c,d,e]	**3p**
$F_{j,0}$	0.0193	0.98	0.98	0.070	0.000	0.005	1.00	1.00
$F_{j,1}$	0.921	0.02	0.02	0.105	0.010	0.863	0.00	0.00
$F_{j,2}$	0.0571	0.00	0.00	0.078	0.890	0.128	0.00	0.00
$F_{j,3}$	0.0028	0.00	0.00	0.427	0.100	0.003	0.00	0.00
$F_{j,4}$	0.000	0.00	0.00	0.250	0.000	0.001	0.00	0.00
$F_{j,5}$	0.000	0.00	0.00	0.103	0.000	0.000	0.00	0.00
$F_{j,6}$	0.000	0.00	0.00	0.024	0.000	0.000	0.00	0.00

For Ne: 1s:[a], Landers *et al* [63]; similar experimental data (differences within 2%) can be found in Morgan *et al* [64], Saito *et al* [65] and Carlson *et al* [57] (the latter corrected to exclude L-shell ionization); **2s** and **2p:**[b], theoretical shake-off contribution [58, 66]. $F_{2s,1} \approxeq 0.03$–0.06 has been suggested by Schmidt *et al* [67].
For Ar: 1s: [c] Carlson *et al* [49]; **2s** and **2p:** [d] Brünken *et al* [68]; similar values for 2p-photoionization have been reported by Viefhaus *et al* [69]; **3s:** different works, [c] Carlson *et al* [49], [d] Brünken *et al* [68] and recently [e] Karamatskos *et al* [70].

Table 3. Branching ratios for multiple ionization of Kr. Notation as in table 2.

Kr								
	1s^f	**2s**^{f}	**2p**^{g}	**3s**^{h}	**3p**^{h}	**3d**^{h}	**4s**^{h}	**4p**
$F_{j,0}$	<0.01	0.00	0.00	0.00	0.00	<0.01	1.00	1.00
$F_{j,1}$	0.01	0.00	0.01	<0.02	<0.02	0.670	0.00	0.00
$F_{j,2}$	0.04	<0.01	0.03	0.12	0.623	0.320	0.00	0.00
$F_{j,3}$	0.19	0.02	0.19	0.66	0.333	<0.01	0.00	0.00
$F_{j,4}$	0.21	0.156	0.35	0.21	<0.02	<0.01	0.00	0.00
$F_{j,5}$	0.17	0.30	0.31	0.00	0.00	0.00	0.00	0.00
$F_{j,6}$	0.13	0.35	0.11	0.00	0.00	0.00	0.00	0.00

For Kr: 1s^f El-Shermi *et al* [71] **2s**^{f} El-Shermi *et al* [71]; **2p**^{g} Morishita *et al* [72], other values can be found in Armen *et al* [61] and in El-Shermi *et al* [71]; **3s**^{h} Tamenori *et al* [60]; **3p**^{h} Tamenori *et al* [60], the values displayed are weighted mean values of $3p_{3/2}$ and $3p_{1/2}$; alternative values (differences less than 10%) can be found in Brünken *et al* [68], Matsui *et al* [73] and Armen *et al* [61]; **3d**^{h} Tamenori *et al* [60], other similar data in Brünken *et al* [68] and Saito *et al* [74], recent theoretical values by Zeng *et al* [75] are in good agreement too; **4s, 4p**^{h} Tamenori *et al* [60] show that the energy threshold of Kr^{2+} is above $Kr^+(4s^{-1})$, so the decay from $Kr^+(4s^{-1})$ to Kr^{2+} is not energetically possible.

Table 4. Similar to 2 and 3 for Xe target.

Xe											
	1s^f	**2s**^{f}	**2p**^{f}	**3s**^{k}	**3p**^{l}	**3d**^{l}	**4s**^{k}	**4p**^{m}	**4d**^{p}	**5s**	**5p**
$F_{j,0}$	<0.01	<0.01	<0.01	0.00	0.00	0.00	0.00	0.00	0.00	1.00	1.00
$F_{j,1}$	0.019	<0.01	<0.01	0.00	0.00	0.00	0.01	0.05	0.80	0.00	0.00
$F_{j,2}$	0.011	<0.01	<0.01	0.003	0.00	0.049	0.165	0.89	0.20	0.00	0.00
$F_{j,3}$	0.043	0.012	0.042	0.007	0.00	0.43	0.774	0.06	0.00	0.00	0.00
$F_{j,4}$	0.058	0.035	0.035	0.024	0.13	0.32	0.051	0.00	0.00	0.00	0.00
$F_{j,5}$	0.114	0.068	0.063	0.126	0.27	0.17	0.00	0.00	0.00	0.00	0.00
$F_{j,6}$	0.143	0.104	0.097	0.426	0.43	0.028	0.00	0.00	0.00	0.00	0.00

For Xe: 1s^f El-Shermi *et al* [71]; **2s**^{f} El-Shermi *et al* [71]; **2p**^{f} El-Shermi *et al* [71]; **3s** and **4s**^{k} Kochur *et al* [76], theoretical calculation; no experimental data available; **3p**^{l} Saito and Suzuki [77]; **3d**^{l} Saito and Suzuki [77]; similar experimental values have been reported in [78]; also in agreement with differential data for $3d_{5/2}$ initial vacancy in [73, 78, 79]. **4p**^{m} Hikosaka *et al* [80]; the theoretical results by Kochur *et al* [76] are in good agreement with these experimental values; **4d**^{p} Hayaishi *et al* [81] and Kämmerling *et al* [82]; the Xe N-shell values by Carlson *et al* [49] include O-shell ionization and are not presented in this table.

which are quite close to recent values by Tamenori *et al* [60] and Armen *et al* [61]).

In tables 2, 3 and 4 we display the branching ratios used in this work for PCI of 0–6 electrons and all the shells of Ne, Ar, Kr and Xe. These values have already been employed with good results in previous calculations of MI of rare gases by protons, antiprotons and different positive ions [34–38, 62]. A detailed discussion on the experimental branching ratios and the comparison of the different data available in the literature is included in [37]. This review has been updated and completed in the present contribution. For example in tables 3 and 4 we display the data for the deepest shells of Kr and Xe. The importance of these contributions in MI is analysed in Tavares *et al* [36].

The selection criteria for the branching ratios takes into account the latest experimental techniques, coincident measurements, the comparison between experimental and theoretical values, and the convergence of the data around a certain value. Only in two cases, 3s and 4s initial vacancies of Xe, no experimental values were found so we include in table 4 the theoretical results by Kochur *et al* [76]. In this respect, it should be mentioned that the calculated branching ratios for Xe by Kochur *et al* [76] for the other sub-shells are in good agreement with the experimental ones displayed in table 4.

A point of discussion is the possibility of PCI following the initial ionization of a valence electron [38]. Auger emission after ionization of the *ns*-subshell (with *n* being the quantum number of the valence shell) is not energetically possible, even when there are six outer electrons in the *np*-subshell [83]. Very recently Karamatskos *et al* [70] underlined this by saying that Ar with a 3s vacancy is a no autoionizing state (only spontaneous radiative decay is possible). This is expressed as $F_{n,i} = \delta_{i,0}$ (no electron is emitted in PCI) in the last two columns of tables 2, 3 and 4.

However the discussion of other possible mechanisms (non-Auger) of second electron emission in valence shell ionization is open, for example shake-off processes due to the change in the target potential [58, 59, 66, 84], or interatomic Coulomb decay in dimers [85–88].

The case of Ne, the lowest Z target considered here, it is different from the others in many aspects. Not considering the valence shell leaves only the K-shell as a source of PCI. In practice, we found that above 1 keV the double ionization cross section of Ne cannot be explained by direct double ionization or by K-shell ionization followed by PCI [37, 38] of one more electron. This may be an indirect evidence of PCI following valence-shell ionization for this atom. Following [38], we include PCI after L-shell ionization of Ne by using the branching ratios for Ne 2s and 2p displayed in table 2. These values are based on shake-off calculations by Mukoyama *et al* [66], as explained in [38]. This must be considered an alternative approach to this subject, which remains open to further research.

3. Results and discussions

We present our theoretical results for MI of rare gases by electron-impact in the intermediate to high energy range, i.e. electron-impact energies above AE up to 10 keV. These values were obtained by using the CDW-EIS and the first Born approximations equally, both corrected for light-particle impact as described in the previous section. The convergence of the CDW-EIS results to the first Born ones at high energies was clearly noted. Thus, we expanded the calculations above 600 eV just using the first Born approximation.

The results of the present theoretical proposal to take into account light-particle physics are summarized in figures 2–11. Figures 2–7 show our values for single to sextuple ionization of rare gases, for both, direct and total (direct+PCI) ionization cross sections. Figures 8–11 display our total (or gross) ionization cross sections including PCI. All the figures show the CDW-EIS results for impact energy 20–550 eV, and extend them from 550 eV to 10 keV by using the first Born approximation. We marked this change with a vertical dotted line in all the figures.

The test of the present method was performed by comparing with an extensive amount of electron-impact data. In general, the MI measurements are relative multiple to single. Absolute values were obtained by measuring total or single

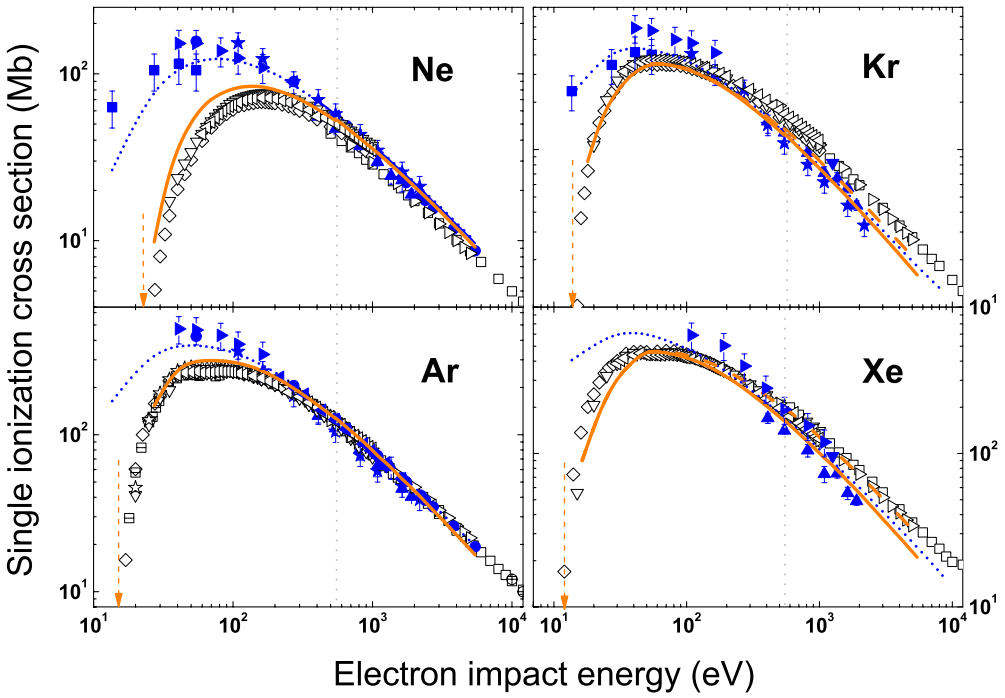

Figure 2. Single ionization cross sections of Ne, Ar, Kr and Xe by electron and by proton-impact. Curves: present results for electron-impact direct ionization (orange dashed-line) and for total single ionization (direct + PCI) (orange solid-line); present results for proton-impact ionization including PCI (blue dotted-line); vertical arrow, AE by [46, 47]. Experimental data: **for electron-impact**, □ Schram *et al* [9], ▷ Nagy *et al* [12], ▽ Krishnakumar *et al* [13], ◯ Syage [14], ◊ Rejoub *et al* [15], ⊟ McCallion *et al* [16], ◁ Kobayashi *et al* [17], hollow ⋆ Straub *et al* [18], ⊖ Almeida *et al* [19], ⊞ Liebius *et al* [20], cross-circle 10 keV value by Singh *et al* [21]; **for proton-impact**, ■ DuBois [89]; ★ DuBois *et al* [90], ● Andersen *et al* [91], ▲ Cavalcanti *et al* [33, 92], ▼ Haugen *et al* [93], ◄ Gonzalez *et al* [94], ► for Ne, Ar and Kr Sarkadi *et al* [95], ► for Xe Manson and DuBois [96].

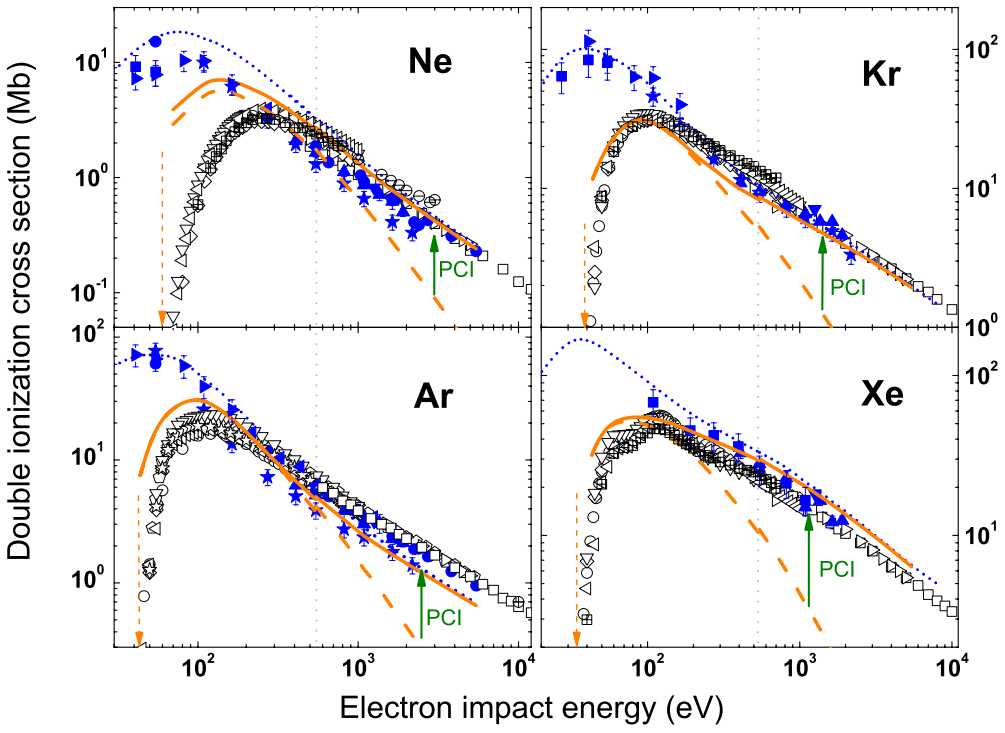

Figure 3. Double ionization cross sections of Ne, Ar, Kr and Xe by electron and proton-impact. Curves and symbols as in figure 2.

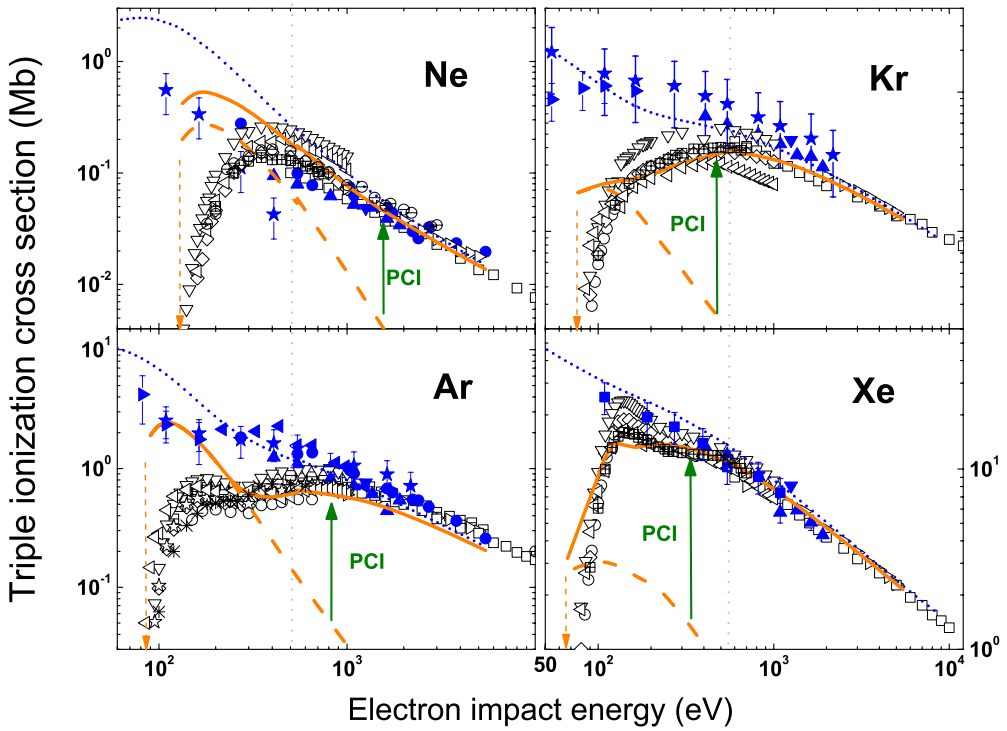

Figure 4. Triple-ionization cross sections of Ne, Ar, Kr and Xe by electron and proton-impact. Curves and symbols as in figure 2, plus ✳ Koslowski *et al* [22].

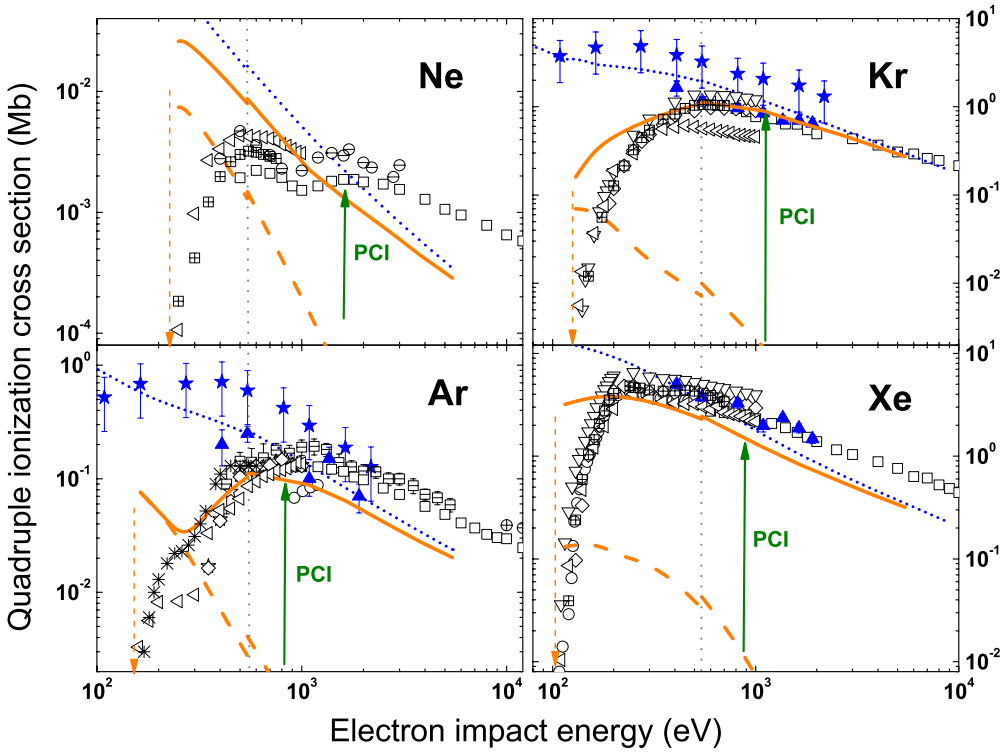

Figure 5. Quadruple-ionization cross sections of Ne, Ar, Kr and Xe by electron and proton-impact. Curves as in figure 2. Experimental data: **for electron-impact**, □ Schram *et al* [9], ▽ Krishnakumar *et al* [13], ◯ Syage [14], ◊ Rejoub *et al* [15], ⊟ McCallion *et al* [16], ◁ Kobayashi *et al* [17], hollow ⋆ Straub *et al* [18], ⊖ Almeida *et al* [19], ⊞ Liebius *et al* [20], cross-circle 10 keV value by Singh *et al* [21], ✳ Koslowski *et al* [22]; **for proton-impact**, ★ DuBois *et al* [90], ▲ Cavalcanti *et al* [92].

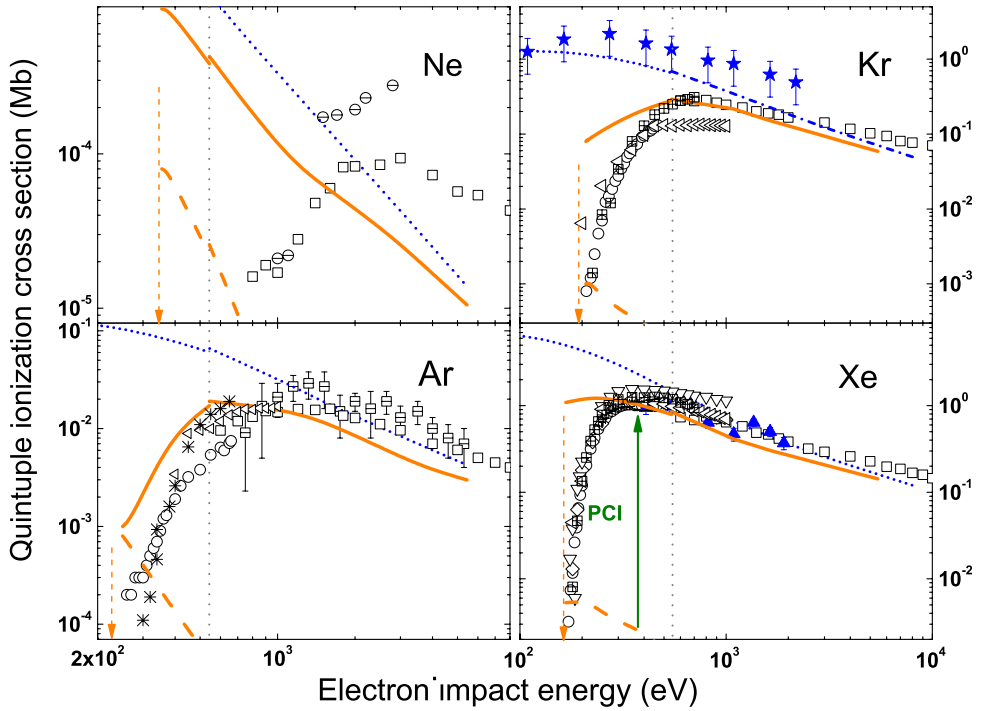

Figure 6. Quintuple-ionization cross sections of Ne, Ar, Kr and Xe by electron and proton-impact. Curves as in figure 2. Experimental data: **for electron-impact**, □ Schram *et al* [9], ▽ Krishnakumar *et al* [13], ◯ Syage [14], ◊ Rejoub *et al* [15], ⊟ McCallion *et al* [16], ◁ Kobayashi *et al* [17], ⊖ Almeida *et al* [19], ⊞ Liebius *et al* [20], ✳ Koslowski *et al* [22]; **for proton-impact**, ★ DuBois *et al* [90], ▲ Cavalcanti *et al* [92].

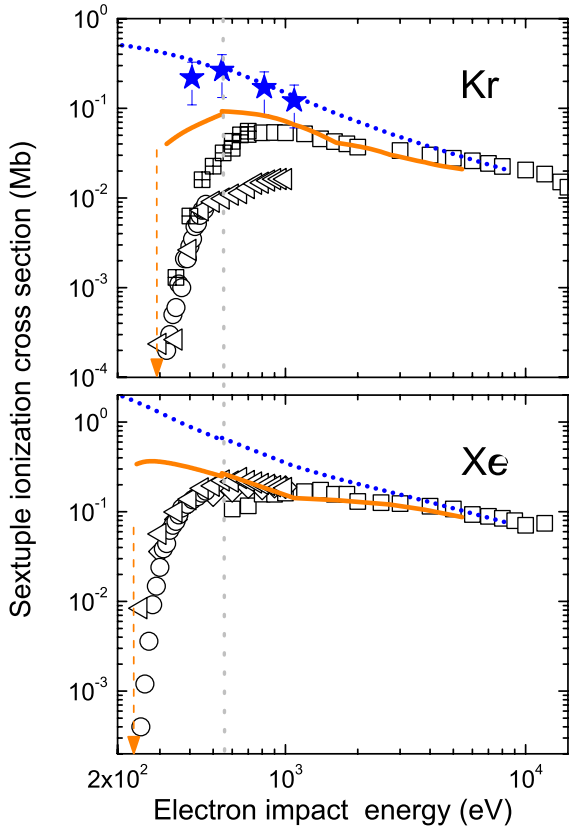

Figure 7. Sextuple-ionization cross sections of Kr and Xe by electron impact. Curves as in figure 2. Experimental data: **for electron-impact**, □ Schram *et al* [9], ◯ Syage [14], ◊ Rejoub *et al* [15], ◁ Kobayashi *et al* [17], ⊞ Liebius *et al* [20]; **for proton-impact**, ★ DuBois *et al* [90].

ionization too. The experimental data available in the literature are absolute cross sections [9–12, 15, 18], or relative ones [13, 16, 17] normalized with well known total ionization cross sections like those by Rapp and Englander-Golden [50], or by Schram *et al* [10].

We have also tested present electron-impact results by comparing them with proton-impact data and with our previous proton-impact results [38]. This represents a high energy proof, but also highlights the changes from the heavy to the light-particle description.

Our CDW-EIS and first Born calculations include all the shells of Ne and Ar, L–M–N shells of Kr and M–N–O shells of Xe. This is important because even though inner-shells may have very small ionization cross sections, their contribution to multiple is important due to cascade Auger processes [36]. We verified that the deeper sub-shells included here (2s of Kr and 3s of Xe) are actually small contributions even in sextuple ionization, and no deeper orbitals are needed.

3.1. Multiple-ionization cross sections including PCI

Figure 2 shows the **single ionization** cross sections together with the experimental data available. The most important feature of this figure is that electron-impact data is quite below the proton-impact values at intermediate energies, and that our theoretical curves agree quite well with them. This shows that our goal has been achieved at this level. The drastic fall down of the values below 100 eV is mainly due to the energy cut off described in 2.1.3.

Our results for Ne and Ar at high energies correctly describes the electron-impact and also the proton-impact

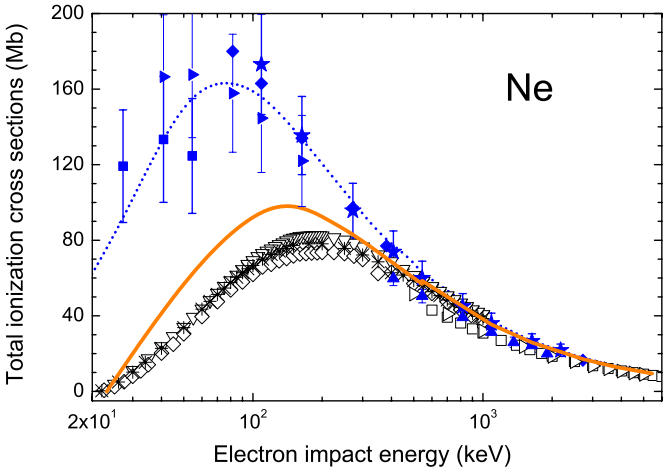

Figure 8. Total ionization cross section of Ne by electron and proton-impact. Curves, present results for gross cross sections including PCI, by electron-impact (orange solid-line), and by proton-impact (blue dotted-line). Experimental data: **for electron-impact**, □ Schram *et al* [10], ⁕ Rapp and Eglander-Golden [50], ▷ Nagy *et al* [12], ▽ Krishnakumar *et al* [13], ◊ Rejoub *et al* [15]; **for proton-impact**, ■ DuBois [89], ★ DuBois *et al* [90], ♦ Rudd *et al* [97], ▲ Cavalcanti *et al* [33], ► Sarkadi *et al* [95].

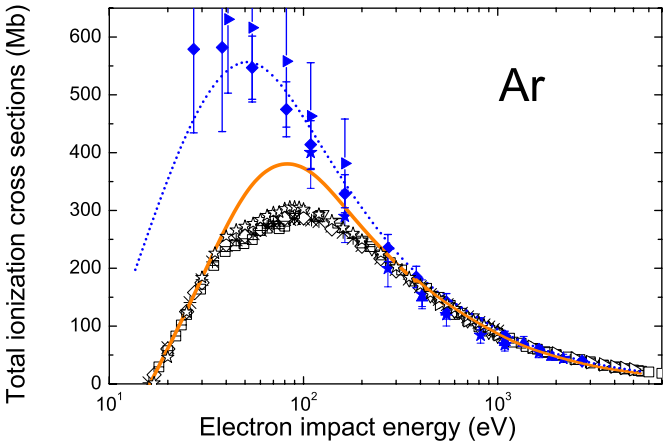

Figure 9. Total ionization cross section of Ar by electron and proton-impact. Curves as in figure 8. Experimental data: **for electron-impact**, □ Schram *et al* [10], ⁕ Rapp and Eglander-Golden [50], ▷ Nagy *et al* [12], ▽ Krishnakumar *et al* [13], ◊ Rejoub *et al* [15], hollow ⋆ Straub *et al* [18], ⊟ McCallion *et al* [16], ◯ Syage [14], ⊠ Sorokin *et al* [54] (count cross sections); **for proton-impact**, ★ DuBois *et al* [90], ♦ Rudd *et al* [97], ▲ Cavalcanti *et al* [92], ► Sarkadi *et al* [95].

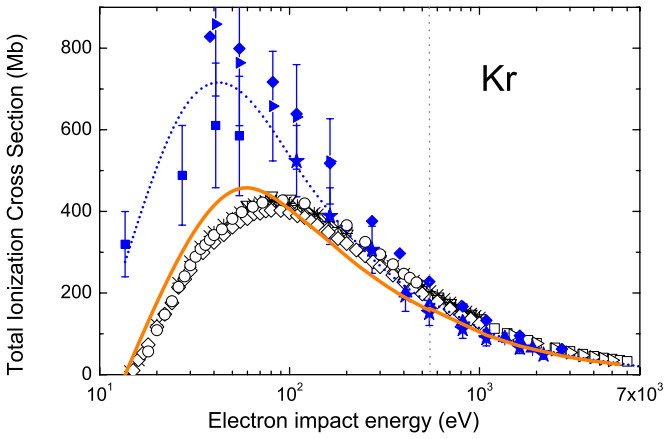

Figure 10. Total ionization cross section of Kr by electron and proton-impact. Curves as in figure 8. Experimental data: **for electron-impact**, □ Schram *et al* [10], ⁕ Rapp and Eglander-Golden [50], ▷ Nagy *et al* [12], ▽ Krishnakumar *et al* [13], ◊ Rejoub *et al* [15], ◯ Syage [14]; **for proton-impact**, ■ DuBois [89], ★ DuBois *et al* [90], ♦ Rudd *et al* [97], ▲ Cavalcanti *et al* [92], ► Sarkadi *et al* [95].

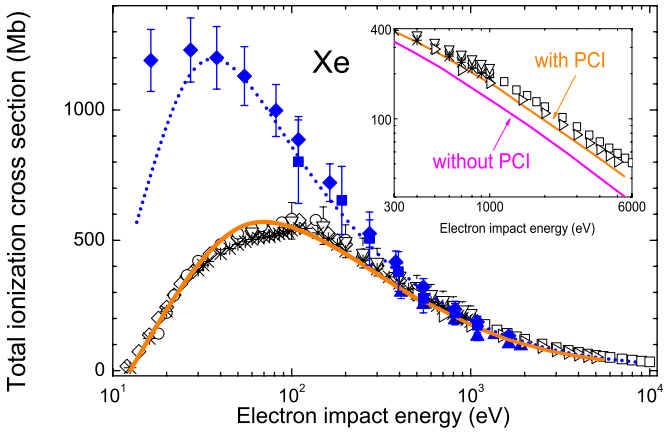

Figure 11. Total ionization cross section of Xe by electron and proton-impact. Curves as in figure 8. Experimental data: for electron-impact, □ Schram *et al* [10], ⁕ Rapp and Eglander-Golden [50], ▷ Nagy *et al* [12], ▽ Krishnakumar *et al* [13], ◊ Rejoub *et al* [15], ◯ Syage [14]; for proton-impact, ▲ Cavalcanti *et al* [92], ♦ Rudd *et al* [97], ■ Manson *et al* [96]. Inset: high energy gross cross sections, with and without PCI.

experimental data. However, for Kr and Xe, our curves underestimate the electron-impact data above 1 keV, being closer to the proton-impact values. Note in figure 2 that for Kr and Xe an experimental discrepancy can be observed between high energy proton and electron impact data. On the other hand, in single ionization, the difference between direct and direct+PCI curves is almost negligible. It can be noted only for Kr and Xe as a small reduction of direct single ionization values because part of them end up as multiple.

At low impact energies the electron–electron correlation is important. We use IPM so we do not expect the present results to describe the ionization processes as we approach the AE region. We decided to mark the suggested AE values by Gstir *et al* [46] and Denifl *et al* [47] with a vertical arrow in figures 2–7.

For **double ionization** our theoretical results and the experimental data available for electron and proton-impact are displayed in figure 3. The comparison shows a good approximation to the picture of the double ionization by electron-impact, except for Ne at low energies. The importance of PCI is very clear in all the cases and the agreement is good in general. Note that the values for Ne include PCI after single ionization of the valence shell as mentioned in 2.3. Details about this contribution are displayed in figures 3 and 4 of [38]. For the electron in Ar at 2 keV, the direct double ionization cross section is a factor 4 below our total cross section including direct and PCI. However, this value is still 25% below the experimental data. This small undervalue for

Ar at high energies may be an effect similar to the case of Ne [88]. On the other hand, the overestimation at low energies (Ne below 400 keV, Ar below 100 keV) is closely related to the minimal cutoff discussed in 2.1.5.

In figure 4 we present our results for **triple ionization** cross sections. In the high energy region the curves for triple ionization including PCI show very good agreement with the experimental data for the four targets, with the contribution of PCI for the heaviest targets being one order of magnitude greater than direct triple ionization. This behaviour is also found and reinforced for higher ionization orders.

At intermediate energies, the electron-impact description shows the correct tendency within the limitations of the present approach. The experimental AE [46, 47] is not well described and the data falls more steeply than the theory, as already mentioned. Note that in the eikonal approximation the projectile velocity is considered constant all along the path. This imposes a serious limitation to treat ionization by low energy electron-impact. The removal of a bound electron is at the expense of the kinetic energy of the projectile, at low impact-energies it accounts for a substantial fraction of the projectile kinetic energy.

We found a two-maximum structure present in both, the triple ionization data and the theoretical curve for Ar, Kr and Xe, though very overestimated in the case of Ar. It is an interesting feature, because this structure is evidence of the entrance of the PCI contribution, which becomes important above a certain energy [22]. The electron-impact experiments displayed in figure 4 show this clearly. A similar structure has been found in MI of positive ions [29].

The results for **quadruple ionization** displayed in figure 5 underline the importance of including PCI, which is the uppermost contribution at high energies. Although the present proposal can be considered a first approach to this subject, the difference with the results just considering direct MI is several orders of magnitude from the experimental values (i.e. at 5 keV, the cross section of direct quadruple ionization of Xe is 4-orders of magnitude below the data). Again, Ar values show a structure around 200–300 eV (direct to PCI region) and the theoretical results too, but highly overestimated. The quadruple ionization of Ne shows the limitations of the present proposal within the IPM.

For Kr our results are much better. Also for Xe, though at impact energies above 1 keV the quadruple ionization of Xe is half of the value expected by Schram [9]. It is important to mention that all the relevant sub-shells were considered in our theoretical calculations. Any difference may come from different branching ratios. However, the data available in the literature to date (references in table 4) support these values.

It can also be noted in figure 6 the importance of PCI in Xe even at the lowest energies considered here (separate direct and direct plus PCI curves). This agrees with the suspicion of Gstir *et al* [46] that the low energy experimental exponent for Xe^{+4} formation, i.e. $p = 3.05$, can be read as triple ionization and PCI of one more electron.

Similar behaviour is observed for the **quintuple ionization** cross sections in figure 6. Note that above 600 eV the curves are first Born approximation results including PCI, which gives a good high energy description of the electron-impact quintuple ionization, for Ar, Kr and Xe. Ne again escapes the rule blatantly. The comparison with proton-impact values for Ne and Ar is only theoretical, no measurements have been reported.

In figure 7 we present surprisingly good results if one considers that they are **sextuple ionization** cross sections for Kr and Xe. For electron impact above 400 eV, the sextuple ionization cross section is mainly single ionization of the inner-shell followed by PCI. The good agreement with the experimental data is sustained in the present theoretical results for the ionization probabilities of the L and M-shells and in the empirical branching ratios for these deep-shells [71, 72, 77].

Two points should be mentioned, first, that the good results for sextuple ionization cross sections displayed in figure 7 above 600 eV are first Born approximation; second, that the only data available above 1 keV were published by Schram *et al* [9], and were measured almost 50 years ago, being nicely described by the present theoretical results. In fact, Schram *et al* [9] measured multiple charged ions Kr^{q+} with $q \leqslant +9$, and Xe^{q+} with $q \leqslant +13$. As far as the IPM is valid, the present formulation can account for higher ionization orders. New experimental data, not only for electron-impact but also for proton-impact, could validate the theoretical effort required for such calculations.

We do not present results for sextuple ionization of Ne and Ar. The latter because there is only one set of experimental data, by Koslowski *et al* [22], but the energy range is somewhat low for our model. No experimental data was found for Ne, and no expectations of the IPM to be valid for these targets so highly ionized.

3.2. Total ionization cross sections including PCI

In figures 8, 9, 10 and 11 we display the present results for the total ionization cross sections given by (16). While performing these calculations we checked that $\sum_{nlm} \sigma_{nlm} = \sum_k k\ \sigma_k < \sum_k k\ \sigma_k^{\mathrm{PCI}}$ and that $\sum_k \sigma_k = \sum_k \sigma_k^{\mathrm{PCI}}$ for each target.

We include in these figures the experimental total ionization cross sections by Schram [10] and by Rapp and Englander-Golden [50], and also the gross cross sections $\sigma_{\mathrm{Total}}^{\mathrm{exp}} = \sum\ n\ \sigma_n^{\mathrm{exp}}$ obtained from the MI measurements reported in [12–16]. Instead, we have not included the accurate experimental data by Sorokin *et al* [54, 55] because they are count cross sections (see section 2.2 for details).

The main result of these four figures is that our electron-impact values have the correct tendency, showing that the changes introduced to take into account light-particle physics were successful. Agreement for all the targets was good above 200 eV and the tendency to proton-impact values at high impact velocities was verified. Again, our results are much better for Kr (differences less than 5%) or Xe than for Ar or Ne, which are overestimated in 25% around the maximum of the cross sections.

It is worth noting that the total cross sections displayed in figures 8, 9, 10 and 11 include PCI. Usually total ionization cross sections are calculated as $\sigma_{\mathrm{gross}} = \sum_{nlm} \sigma_{nlm}$ [7]. This may be valid for low to intermediate charged targets, for

which post-collisional MI is not so important. For example, for Ne and Ar the difference in the total cross sections with or without PCI is less than 5% [38]. Conversely, for Kr and Xe, this difference goes from 20% to 35% [38]. The good agreement we obtained for Kr and Xe at high energies would not have been achieved if PCI had not been included. This is stressed in figure 11 where we included an inset in logarithmic scale to highlight the high energy behaviour and the differences between the total cross sections with PCI ($\sigma_{\rm gross}^{\rm PCI}$) or without PCI ($\sum_{nlm}\sigma_{nlm}$). This difference would be larger if we extended the calculations to higher energies.

This underestimation of the Kr and Xe total ionization cross sections obtained as $\sum_{nlm}\sigma_{nlm}$ at high energies has been known for more than 40 years. In 1977 McGuire [53] carried out a first approximation to the inclusion of PCI of inner-shells with a weighted addition of cross sections of different sub-shells.

On the other hand, at high energies we found that the measurements by Sorokin *et al* [54, 55] are nicely described by count cross sections obtained with the first Born approximation [38]. We should again stress the gross-count difference, which increases with the target atomic number [52].

4. Conclusions

In this contribution we present theoretical calculations of electron impact multiple ionization of Ne, Ar, Kr and Xe by using the CDW-EIS and the first Born approximations adapted from antiproton to electron-impact physics. Our results include the direct or collisional contributions and also the post-collisional ionization. The latter in a semi-empirical way by employing experimental branching ratios of final target charge states after single photoionization.

Present theoretical developments give a reasonable description of the experimental data of multiple ionization (single to sextuple) above the energy where the post-collisional ionization dominates. In the intermediate energy region the correct tendency of the electron impact data both in multiple and in total ionization cross sections was obtained. This shows that the changes introduced to take into account light-particle physics were successful. However, our approximation fails at the energy threshold for multiple ionization.

The results presented here are much better for Kr or Xe than for Ne or even for Ar. We found a recursive problem in the description of Ne, which became worse for highly ionized final states. Different explanations may be tended, among them the validity of an independent electron model.

We overestimated the q-fold ionization at intermediate to low energies. This is not a low energy model, however improvements may be expected by considering a more realistic energy cutoff for the multiple ionization.

We also calculated total ionization cross sections and showed that the post-collisional ionization also affects the total ionization too. This influence is negligible for Ne or even Ar, but increases with target atomic number, being 25% for Kr at 5 keV and 37% for Xe.

The methodology followed here for multiple ionization including PCI could be combined with any alternative model for the electron impact ionization probabilities as function of the impact parameter.

Acknowledgments

This work was partially supported by the following Argentinean institutions: Consejo Nacional de Investigaciones Científicas y Técnicas, Agencia Nacional de Promoción Científica y Tecnológica, and Universidad de Buenos Aires.

References

[1] Shevelko V and Tawara H 1998 *Atomic Multielectron Processes* (Berlin: Springer-Verlag)
[2] Bartlett P L and Stelbovics A T 2010 *Nucl. Instrum. Methods Phys. Res.* B **619** 1
[3] Bartlett P L 2006 *J. Phys. B: At. Mol. Opt. Phys.* **39** R379
[4] Pindzola M S *et al* 2007 *J. Phys. B: At. Mol. Opt. Phys.* **40** R39
[5] Fernandez-Varea J M, Segui S and Dingfelder M 2011 *Phys. Rev.* A **83** 022702
[6] Segui S, Dingfelder M and Salvat F 2003 *Phys. Rev.* A **67** 062710
[7] Bartlett P L and Stelbovics A T 2002 *Phys. Rev.* A **66** 012707
[8] Popov Y V, Chuluunbaatar O, Shablov V L and Kouzakov K A 2010 *Phys. Part. Nucl.* **41** 543–73
[9] Schram B L, Boerboom A J H and Kistermaker J 1966 *Physica* **32** 185–96
Schram B L 1966 *Physica* **32** 197–209
[10] Schram B L, de Heer F J, Van der Wiel M J and Kistermaker J 1965 *Physica* **31** 94
[11] Adamczyk B, Boerboom A J H, Schram B L and Kistermaker J 1966 *J. Chem. Phys.* **44** 4640–2
[12] Nagy P, Skutlartz A and Schmidt V 1980 *J. Phys. B: At. Mol. Opt. Phys.* **13** 1249–67
[13] Krishnakumar E and Srivastava S K 1988 *J. Phys. B: At. Mol. Opt. Phys.* **21** 1055–82
[14] Syage J A 1992 *Phys. Rev.* A **46** 5666
[15] Rejoub R, Lindsay B G and Stebbing R F 2002 *Phys. Rev.* A **65** 042713
[16] McCallion P, Shah M B and Gilbody H B 1992 *J. Phys. B: At. Mol. Opt. Phys.* **25** 1061–71
[17] Kobayashi A, Fujiki G, Okaji A and Masuoka T 2002 *J. Phys. B: At. Mol. Opt. Phys.* **35** 2087–103
[18] Straub H C, Renault P, Lindsay B G, Smith K A and Stebbings R F 1995 *Phys. Rev.* A **52** 1115–24
[19] Almeida D P, Fontes A C and Godinho C F L 1995 *J. Phys. B: At. Mol. Opt. Phys.* **28** 3335–45
[20] Liebius H, Binder J, Koslowwski H R, Wiesemann K and Huber B A 1989 *J. Phys. B: At. Mol. Opt. Phys.* **22** 83–97
[21] Singh R K, Hippler R and Shanker R 2002 *J. Phys. B: At. Mol. Opt. Phys.* **35** 3243–56
[22] Koslowski H R, Binder J, Huber B A and Wiesemann K 1987 *J. Phys. B: At. Mol. Opt. Phys.* **20** 5903
[23] Pindzola M S, Loch S D, Borovik A Jr, Gharaibeh M F, Rudolph J K, Schippers S and Müller A 2013 *J. Phys. B: At. Mol. Opt. Phys.* **46** 215202
[24] Lecointre J, Kouzakov K A, Belic D S, Defrance P, Popov Y V and Shevelko V P 2013 *J. Phys. B: At. Mol. Opt. Phys.* **46** 205201
[25] Lecointre J, Jureta J J and Defrance P 2008 *J. Phys. B: At. Mol. Opt. Phys.* **41** 095204
[26] Fisher V, Ralchenko Y, Goldgirsh A, Fisher D and Maron Y 1995 *J. Phys. B: At. Mol. Opt. Phys.* **28** 3027–46
[27] Deutsch H, Becker K, Matt S and Märk T D 1998 *Plasma Phys. Control. Fusion* **40** 1721

[28] Shevelko V P and Tawara H 1995 *J. Phys. B: At. Mol. Opt. Phys.* **28** L589
[29] Shevelko V P, Tawara H, Scheuermann F, Fabian B, Müller A and Salzborn E 2005 *J. Phys. B: At. Mol. Opt. Phys.* **38** 525
[30] Jha L K, Kumar S and Roy B N 2006 *Eur. Phys. J.* D **40** 101–6
[31] Salop A 1973 *Phys. Rev.* A **8** 3032
[32] Spranger T and Kirchner T 2004 *J. Phys. B: At. Mol. Opt. Phys.* **37** 4159
[33] Cavalcanti E G, Sigaud G M, Montenegro E C, Sant 'Anna M M and Schmidt-Bocking H 2002 *J. Phys. B: At. Mol. Opt. Phys.* **35** 3937
[34] Montanari C C, Wolff W, Luna H, Santos A C F, Montenegro E C and Miraglia J E 2012 Multiple ionization of atoms including post-collisional contributions *Proc. 27th Int. Conf. on Photonic, Electronic and Atomic Collisions 2011 Belfast; J. Phys: Conf. Ser.* **388** 012036
[35] Wolff W, Luna H, Santos A C F, Montenegro E C, DuBois R D, Montanari C C and Miraglia J E 2011 *Phys. Rev.* A **84** 042704
[36] Tavares A C, Montanari C C, Miraglia J E and Sigaud G M 2014 *J. Phys. B: At. Mol. Opt. Phys.* **47** 045201
[37] Montanari C C, Montenegro E C and Miraglia J E 2010 *J. Phys. B: At. Mol. Opt. Phys.* **43** 165201
[38] Montanari C C and Miraglia J E 2012 *J. Phys. B: At. Mol. Opt. Phys.* **45** 105201
[39] Fainstein P D, Ponce V H and Rivarola R D 1988 *J. Phys. B: At. Mol. Opt. Phys.* **21** 287–99
[40] Rivarola R D, Fainstein P D and Ponce V H 1989 *AIP Conf. Proc. XVI Int. Conf. on the Physics of Electronic and Atomic Collisions* vol 405, ed A Dalgarno *et al* (New York: AIP) p 264
[41] Galassi M E, Rivarola R D and Fainstein P D 2007 *Phys. Rev.* A **75** 052708
[42] Salvat F, Fernandez-Varea J M and Williamson W Jr 1995 *Comput. Phys. Comm.* **90** 151
[43] Aashamar K, Luke T M and Talman J D 1979 *J. Phys. B: At. Mol. Opt. Phys.* **12** 3455
[44] Guire M 1982 *Phys. Rev. Lett.* **49** 1153
[45] Lahmam-Bennani *et al* 2010 *J. Phys. B: At. Mol. Opt. Phys.* **43** 105201
[46] Gstir B *et al* 2002 *J. Phys. B: At. Mol. Opt. Phys.* **35** 2993
[47] Denifl S *et al* 2002 *J. Phys. B: At. Mol. Opt. Phys.* **35** 4685
[48] Liu Y, Zeng J and Yuan J 2013 *J. Phys. B: At. Mol. Opt. Phys.* **46** 145002
[49] Carlson T A, Hunt W E and Krause M O 1966 *Phys. Rev.* **151** 41
[50] Rapp D and Englander-Golden P 1965 *J. Chem. Phys.* **43** 1464
[51] Tawara H and Kato T 1987 *At. Data Nucl. Data Tables* **36** 167
[52] de Heer F J, Jansen R H J and van der Kaay W 1979 *J. Phys. B: At. Mol. Opt. Phys.* **12** 979–1002
[53] McGuire E J 1971 *Phys. Rev.* A **3** 267
McGuire E J 1977 *Phys. Rev.* A **16** 62
[54] Sorokin A A, Shmaenok L A, Bobashev S V, Möbus B, Richter M and Ulm G 2000 *Phys. Rev.* A **61** 022723
[55] Sorokin A A, Shmaenok L A, Bobashev S V, Möbus B and Ulm G 1998 *Phys. Rev.* A **58** 2900
[56] Krause M O and Carlson T A 1966 *Phys. Rev.* **149** 52
[57] Carlson T A and Krause M O 1965 *Phys. Rev.* **140** A1057
[58] Carlson T A and Nestor C W Jr 1973 *Phys. Rev.* A **8** 2887–93
[59] Carlson T A, Nestor C W Jr, Tucker T C and Malik F B 1968 *Phys. Rev.* **169** 27–36
[60] Tamenori Y, Okada K, Tanimoto S, Ibuki T, Nagaoka S, Fujii A, Haga Y and Suzuki I H 2004 *J. Phys. B: At. Mol. Opt. Phys.* **37** 117
[61] Armen G B, Kanter E P, Krässig B, Levin J C, Southworth S H and Young L 2004 *Phys. Rev.* A **69** 062710
[62] Archubi C D, Montanari C C and Miraglia J E 2007 *J. Phys. B: At. Mol. Opt. Phys.* **40** 943
[63] Landers A L *et al* 2009 *Phys. Rev. Lett.* **102** 223001
[64] Morgan D V, Sagurton M and Bartlett R J 1997 *Phys. Rev.* A **55** 1113
[65] Saito N and Suzuki I H 1992 *Phys. Scr.* **45** 253
[66] Mukoyama T and Taniguchi K 1987 *Phys. Rev.* A **36** 693–8
[67] Schmidt V, Sandner N, Kuntzemüller H, Dhez P, Wuilleumier F and Källne E 1976 *Phys. Rev.* A **13** 1748
[68] Brünken S, Gerth C, Kanngieber B, Luhmann T, Richter M and Zimmermann P 2002 *Phys. Rev.* A **65** 042708
[69] Viefhaus J *et al* 2004 *Phys. Rev. Lett.* **92** 083001
[70] Karamatskos E T, Markellos D and Lambropoulos P 2013 *J. Phys. B: At. Mol. Opt. Phys.* **46** 164011
[71] El-Shermi A, Lofty Y and Zschornack G 1997 *J. Phys. B: At. Mol. Opt. Phys.* **30** 237–50
[72] Morishita Y, Tamenori Y, Okada K, Oyama T, Yamamoto K, Tabayashi K, Ibuki T, Moribayashi K and Suzuki I H 2006 *J. Phys. B: At. Mol. Opt. Phys.* **39** 1323
[73] Matsui T, Yoshii H, Tsukamoto K, Kawakita S, Murakami E, Adachi J, Yagishita A, Morioka Y and Hayaishi T 2004 *J. Phys. B: At. Mol. Opt. Phys.* **37** 3745
[74] Saito N and Suzuki I H 1997 *J. Phys. Soc. Japan* **66** 1979
[75] Zeng J L, Liu P F, Xiang W J and Yuan J M 2013 *J. Phys. B: At. Mol. Opt. Phys.* **46** 215002
[76] Kochur A G, Dudenko A I, Sukhorukov V L and Petrov I D 1994 *J. Phys. B: At. Mol. Opt. Phys.* **27** 1709
[77] Saito N and Suzuki I H 1992 *J. Phys. B: At. Mol. Opt. Phys.* **25** 1785–93
[78] Tamenori Y *et al* 2002 *J. Phys. B: At. Mol. Opt. Phys.* **35** 2799
[79] Partanen L, Sanjari R, Osmekhin S, Hu Z F, Kukk E and Aksela H 2005 *J. Phys. B: At. Mol. Opt. Phys.* **38** 1881–93
[80] Hikosaka Y, Lablanquie P, Penent F, Kaneyasu T, Shigemasa E, Eland J H D, Aoto T and Ito K 2007 *Phys. Rev.* A **76** 032708
[81] Hayaishi T, Yagishita T, Shigemasa E, Murakami E and Morioka Y 1990 *J. Phys. B: At. Mol. Opt. Phys.* **23** 4431
[82] Kärmmerling B, Krassig B and Schmidt V 1992 *J. Phys. B: At. Mol. Opt. Phys.* **25** 3621
[83] Kochur A G, Sukhorukov V L, Dudenko A I and Demekhin Ph V 1995 *J. Phys. B: At. Mol. Opt. Phys.* **28** 387
[84] Kochur A G and Popov V A 2006 *Radiat. Phys. Chem.* **75** 1525–8
[85] Jahnke T *et al* 2004 *Phys. Rev. Lett.* **93** 063401
[86] Marburger S *et al* 2003 *Phys. Rev. Lett.* **90** 203401
[87] Kim H-K 2013 *Phys. Rev.* A **88** 042707
[88] Yan S 2013 *Phys. Rev.* A **88** 042712
[89] DuBois R D 1984 *Phys. Rev. Lett.* **52** 2348–51
[90] DuBois R D, Toburen L H and Rudd M E 1984 *Phys. Rev.* A **29** 70–76
[91] Andersen L H, Hvelplund P, Knudsen H, Möller S P, Sörensen A H, Elsener K, Rensfelt K G and Uggerhöj 1987 *Phys. Rev.* A **36** 3612–29
[92] Cavalcanti E G, Sigaud G M, Montenegro E C and Schmidt-Bocking H 2003 *J. Phys. B: At. Mol. Opt. Phys.* **36** 3087
[93] Haugen H K, Andersen L H, Hvelplund P and Knudsen H 1982 *Phys. Rev.* A **26** 1962–74
[94] Gonzalez A D and Horsdal Pedersen E 1993 *Phys. Rev.* A **48** 3689
[95] Sarkadi L, Herczku P, Kovacs S T S and Kover A 2013 *Phys. Rev.* A **87** 062705
[96] Manson S T and DuBois R D 1987 *J. Phys.* **48** C9 263–6
[97] Rudd M E, Kim Y-K, Madison D H and Gallagher J W 1985 *Rev. Modern Phys.* **57** 965–94